

An integrated workflow for MICP-based rock typing: A case study of a tight-gas sandstone reservoir in the Baltic Basin (Poland)

Metodologia wyznaczania klas podobieństw (*rock types*) w oparciu o dane MICP na przykładzie zwięzłych piaskowców typu *tight-gas* z basenu bałtyckiego

Tomasz Topór

Oil and Gas Institute – National Research Institute

ABSTRACT: One of the most important tasks in the characterization of unconventional tight-gas sandstone reservoirs is a proper evaluation of rock types (RT). Rock typing based on pore structure has a great potential to capture fluctuations in storage potential, and fluid transport within the formations studied. This study presents a newly adapted workflow to formulate rock types in tight-gas sandstone reservoirs based on similarities in pore structure. Rock types are identified using the *k*-means clustering method (unsupervised learning) on pore structure parameters derived from measuring mercury injection capillary pressure (MICP). The parameters associate opened porosity, proportions of macro-, meso-, micro-, and nanopores, and selected MICP-derived permeability. The correlation between pulse decay permeability and permeabilities calculated from MICP analysis revealed that Swanson permeability is the most useful permeability estimation for rock typing. The cluster analysis performed on 178 samples revealed four rock types (RT1–RT4) of unique pore system characteristics that significantly differ in macro-, meso-, micro-, and nanopore content. The clusters' tendency was evaluated using the Hopkins statistic. The optimal number of clusters was determined using the Elbow method as an internal validation technique. Rock types 1 and 2 (RT1 and RT2) showed a highly tight character with a Swanson permeability of <0.1 mD and an opened porosity of $<5\%$. Samples from RT3 and RT4 revealed more conventional characteristics with a Swanson permeability of >0.1 mD and an opened porosity of $>5\%$. The variability in the pore structure between designated rock types was also captured using Computerized Analysis of Microscopic Images (CAMI) on the thin-sections from the most representative samples of the individual rock types. Pore structure characteristics (opened porosity and pore-throat distribution) with Swanson permeability and rock types were integrated into an array log to locate the most perspective intervals within the formation under study.

Key words: tight-gas sandstones, rock typing, MICP, machine learning

STRESZCZENIE: Jednym z kluczowych zadań w charakterystyce niekonwencjonalnych piaskowców typu *tight gas* jest prawidłowe wyznaczenie klas podobieństw, tzw. *rock types*. *Rock typing* oparty na charakterystyce systemu porów posiada duży potencjał wyznaczania stref o pożądanych własnościach zbiornikowych i filtracyjnych w badanej formacji. Praca pokazuje metodologię wyznaczania klas podobieństw na podstawie charakterystyki systemu porów w formacjach zwięzłych piaskowców. Klasy podobieństw zostały wyznaczone za pomocą metody *k*-średnich w oparciu o wyselekcjonowane parametry przestrzeni porowej: porowatość otwartą, frakcje makro-, mezo-, mikro- i nanoporów oraz przepuszczalność Swansona. Wszystkie parametry zostały wyznaczone na podstawie danych MICP. Korelacja pomiędzy przepuszczalnością otrzymaną metodą *pulse decay* i przepuszczalnościami wyliczonymi z MICP pokazała, że najbardziej wiarygodną metodą szacowania przepuszczalności do *rock typingu* jest metoda Swansona. Analiza klastrowa przeprowadzona na 178 próbkach pozwoliła na wyznaczenie 4 typów skał (*rock types* RT1–RT4) cechujących się odmienną charakterystyką systemu porów, w której dominowały makro-, mezo-, mikro- lub nanopory. Tendencja do tworzenia klastrów została oceniona za pomocą metody/statystyki Hopkina. Optymalna liczba klastrów została wyznaczona przy użyciu wewnętrznych metod walidacyjnych (metoda „*elbow*”). Próbki należące do typów 1 i 2 (RT1 i RT2) charakteryzują się silnie zwięzłym charakterem z przepuszczalnością Swansona $<0,1$ mD i porowatością otwartą $<5\%$. Próbki z klas 3 i 4 (RT3 i RT4) posiadają bardziej konwencjonalny charakter z przepuszczalnością Swansona $>0,1$ mD i porowatością otwartą $>5\%$. Zmienność pomiędzy wyznaczonymi klasami została również zaobserwowana w wynikach analizy obrazu mikroskopowego (CAMI), która została wykonana na płytkach cienkich dla najbardziej reprezentatywnych próbek z poszczególnych klas. Zintegrowanie otrzymanych wyników dotyczących struktury porowej (porowatość otwarta, rozkład porów), przepuszczalności Swansona oraz klas podobieństw zostało wykorzystane do wskazania stref o najlepszych własnościach zbiornikowych i filtracyjnych w badanej formacji.

Słowa kluczowe: piaskowce typu *tight-gas*, klasy podobieństwa skał, MICP, uczenie maszynowe.

Corresponding author: T. Topór; e-mail: toport@inig.pl

Article contributed to the Editor: 19.11.2019. Approved for publication: 26.03.2020

Introduction

Substantial natural gas resources and the widespread distribution of tight-gas sandstone formations make them an important global energy resource (Naik, 2005; Ma et al., 2015). Tight-gas sandstone reservoirs are by their nature extensions of conventional sandstone reservoirs, but ones with low permeability (<0.1 mD) and lower effective porosity (Law and Curtis, 2002). Because of the low porosity–permeability structure, the completion techniques for producing tight sandstone reservoirs are often similar to shale-gas reservoirs and require drilling horizontal wells with hydraulic fracturing stimulation. The exploration stage and resource evaluation, however, is quite different (Kennedy et al., 2012).

One of the key tasks in the characterization of tight-gas sandstone reservoirs is a proper evaluation of the rock types within the studied formations (Rushing et al., 2008). The accurate identification of rock types requires an understanding of the local depositional and diagenesis mechanisms that control the physical properties of the rock. Among all rock properties, the pore structure (i.e., pore size, distribution, geometry, etc.) is of great importance for the oil and gas industry because it controls fluid flow and storage potential in all types of reservoirs.

The concept of rock typing has been thoroughly described in the literature, and it is considered to be a best practice for reservoir characterization in various tight-oil and tight-gas formations (Archie, 1950; Amaefule et al., 1993; Rushing et al., 2008; Skalinski et al., 2011; Aliyev et al., 2016; Mirzaei-Paiaman et al., 2018). Many definitions of rock typing exist depending on the classification scheme used, including depositional, petrographic, log-based, or hydraulic (Ma et al., 2015). Among these, hydraulic rock type classification mostly relies on the pore network parameters and provides a physical measure of the rock storage and flow properties at current conditions, as modified by diagenesis (Rushing et al., 2008).

Pore structure attributes such as pore throat size and distribution (PTD), geometry, and specific surface area (SSA) – as determined by mercury injection capillary pressure (MICP) – control the magnitude of permeability for a given rock in the reservoir (Pittman, 1992; Such et al., 2007; Krakowska et al., 2018). Hydraulic rock typing based on dominant pore throat size or its proportions (mega-, macro-, meso-, micro-, and nanopores) has been successfully used in the differentiation of rock types in various reservoir rocks (Skalinski et al., 2011; Skalinski and Kenter, 2014; Aliyev et al., 2016; Rabiller, 2017; Mirzaei-Paiaman et al., 2018). MICP data can also be used to determine permeability and to develop a porosity–permeability relationship (Katz and Thompson, 1987; Pittman, 1992; Comisky et al., 2007; Swanson, 2007; Rabiller, 2017). The most common models incorporate pore dimensions and characteristic

lengths that can be obtained from MICP measurement. Proper hydraulic rock types should integrate all available pore structure information and try to develop a unique porosity–permeability relationship for a given rock type.

This study presents a workflow for a modified hydraulic rock typing using pore structure parameters from MICP analysis to identify different rock types in the Cambrian tight-gas sandstone reservoir from the Baltic Basin (Poland). The rock types were identified using *k*-means clustering and proportions of macro-, meso-, micro-, and nanopores, opened porosity, and MICP-based calculated permeability. The results were used to identify zones within the studied formation of the most promising reservoir parameters that determined the reservoir's storage and flow potential.

Materials and Methods

The data analyzed herein consist of archived, tabulated MICP data and grain density data collected from 186 core/plug samples from a well drilled in the Polish part of the Baltic Basin during recent exploration (2013–2014). The sample-set represents tight-gas sandstones with a present-day depth ranging from 2959–3068 m and representing a Middle Cambrian sandstone formation.

Helium pycnometry and mercury injection capillary pressure (archived data)

The skeletal density of the samples was measured with an AccuPyc II 1340 Series Pycnometer (Micromeritics) using the gas displacement method and helium as the analytical gas. All 184 samples were analyzed after drying the rock chips in an oven at 110°C for 24 h.

The MICP measurements were performed on the same samples as helium pycnometry, using an AutoPore IV 9500 Series Mercury Porosimeter (Micromeritics) with pressure steps from 0 to 30,000 psi, covering a pore throat diameter range of approximately 300 μm to 0.006 μm (6 nm). All MICP data were re-examined in order to recalculate the petrophysical parameters after necessary corrections.

Gas Permeability – pressure pulse-decay (PDP)

The plus-decay technique was used to measure the permeability at simulated reservoir conditions for 31 selected plugs using a Pulse Decay Permeameter-PDP-250 apparatus (CoreLab). One-inch plug samples were dried in an oven at 110°C for 24 h. The samples were placed in a core holder and subjected to a confining stress of 7000 psi. The PDP system saturated the samples to 5000 psi pore pressure using nitrogen as the analytical gas. Before the permeability test, the samples

were kept under the given conditions for 6 h. PDP permeability (kPDP) was calculated from a linear regression performed on the pressure-time data using the last five experimental points (Jones, 1997).

Results and Discussion

Pore structure characteristics for rock typing

Most of the data analysis and visualization were performed using the R language and the R Studio environment for statistical computing (R Core Team, 2018). In the beginning, conformance and compaction corrections were performed for all MICP curves, using Brown's approach (2015). Conformance is to the amount of Hg needed to envelop irregularities on the sample surface. Compaction occurs before intrusion, when pore space is in a vacuum, and Hg exerts pressure outside the sample. Conformance and compaction are most evident below the threshold pressure; both are artifacts and have been recognized as a source of error when computing petrophysical properties based on MICP experimental results (Comisky et al., 2007; Lan et al., 2017). The resulting, corrected pressure data were converted to the pore throat size distribution (PTD) using Washburn's equation (Washburn, 1921). PTD was subdivided into five classes: mega- ($> 10 \mu\text{m}$), macro- ($10\text{--}2 \mu\text{m}$), micro- ($2\text{--}0.5 \mu\text{m}$), meso- ($0.5\text{--}0.1 \mu\text{m}$), and nanopores ($< 0.1 \mu\text{m}$) (Dolson, 2016). Saturation curves were used to obtain the contribution of each pore class to opened porosity. Opened porosity, SSA, and bulk density were recalculated using the

MICP-corrected data and equations provided in Micromeritics's documentation (Webb, 2001). Skeletal density for the total porosity calculation was taken from the helium pycnometry measurements. The pore structure characteristics from the re-examined MICP data created the core information for rock typing.

The opened porosity of the analyzed samples ranges from 0.45% to 7.52%, with a mean value of 2.58% (Table 1). The pore system is dominated by micro- (mean: 54.21%; median: 62.96%) and nanopores (mean: 29.72%; median: 10.76%). The low porosity values and highly micropore-dominated pore system makes the analyzed sample set very tight (Table 1). In such a sample set, rock typing seems to be an essential operation to reveal zones within the formation that have the potential to accumulate and transport reservoir fluids.

The descriptive statistics for the main petrophysical parameters are presented in Table 1. The detailed description of those parameters for individual rock types (RT) will be provided further in the text.

Permeability estimation for rock typing

Previous studies have provided a comprehensive evaluation of permeability models from MICP data (Such and Leśniak, 2003; Comisky et al., 2007; Brown, 2015). In this study, permeability was estimated using three popular models derived from the characteristic length theory (Katz and Thompson's and Swanson's methods) and the Poiseuille theory (Purcell's method) (Purcell, 1949; Katz and Thompson, 1987; Swanson, 2007). The models were applied to all samples except six –

Table 1. Descriptive statistics for the main petrophysical parameters

Tabela 1. Statystyka opisowa dla głównych parametrów petrofizycznych

	n	mean	sd	median	min	max	range	skew	kurtosis	se
Total Porosity [%]	178	2.68	1.73	2.13	0.46	8.26	7.80	1.21	0.77	0.13
Opened Porosity [%]	178	2.58	1.64	2.07	0.45	7.52	7.07	1.17	0.63	0.12
Grain density [g/cm ³]	178	2.67	0.02	2.67	2.64	2.75	0.11	1.01	1.24	0.00
Bulk density [g/cm ³]	178	2.57	0.06	2.58	2.37	2.68	0.31	-0.97	0.98	0.00
Threshold diam. [μm]	178	1.20	1.61	0.60	0.05	8.90	8.85	2.53	6.60	0.12
Threshold press. [psi]	178	467.7	494.4	301.4	20.4	3376.1	3355.8	2.4	7.80	37.1
Surface area [m ² /g]	178	0.32	0.33	0.19	0.04	2.26	2.22	2.58	8.78	0.02
Macro- [%]	178	5.43	17.28	0.00	0.00	76.38	76.38	3.18	8.68	1.30
Meso- [%]	178	10.64	17.06	1.35	0.00	75.85	75.85	2.00	3.64	1.28
Micro- [%]	178	54.21	32.55	62.96	0.00	98.70	98.70	-0.34	-1.43	2.44
Nano- [%]	178	29.72	34.41	10.76	0.00	100.00	100.00	0.93	-0.68	2.58
k Katz-Thompson [mD]	178	0.21	0.78	0.00	0.00	5.87	5.87	4.90	26.07	0.06
k Swanson [mD]	178	0.25	0.93	0.00	0.00	6.22	6.22	4.61	21.76	0.07
k Purcell [mD]	178	0.51	1.88	0.01	0.00	12.82	12.82	4.80	23.99	0.14
k PDP [mD]	31	0.08	0.23	0.01	0.00	1.00	0.99	3.31	9.57	0.04

n – the sample size within this group; sd – the standard deviation; se – the sample standard error

from depths of 2961.88 m, 2973.13 m, 2982.38 m, 2986.70 m, 3005.95 m, and 3045.30 m – which were rejected from the analyses due to the occurrence of cracks.

In the percolation model, flow paths of rock are treated as a statistical random porous medium with variable PTD, where the flow properties are controlled by a single or multiply characteristic length diameters (Comisky et al., 2007). In the Katz–Thompson hydraulic conductivity model, the characteristic lengths are threshold diameter and the diameter at maximum hydraulic conductivity (Katz and Thompson, 1987). The Katz–Thompson permeability was calculated using the following equation:

$$k_{Katz-Thompson} = \left[\frac{1013}{89} \right] L_{h_{max}}^2 \left[\frac{L_{h_{max}}}{L_c} \right] \Phi S L_{h_{max}} \quad (1)$$

where L_c is the threshold diameter (μm), $L_{h_{max}}$ is the diameter with the maximum hydraulic conductivity (μm ; determined as the maximum of the mercury intruded and pore throat diameter cubed), and $\Phi S L_{h_{max}}$ is the fraction of the total porosity filled with mercury at $L_{h_{max}}$.

In Swanson’s model, the characteristic length corresponds to the apex of $(S_{Hg}/P_c)_A$ and represents a pore diameter where all of the major connected pore spaces controlling permeability have been filled with mercury (Swanson, 2007; Brown, 2015). Swanson’s permeability was calculated using the following equation:

$$k_{Swanson} = 399 \left(\frac{S_{Hg}}{P_c} \right)_A^{1.691} \quad (2)$$

where S_{Hg} is the bulk percent of mercury saturation, P_c is the capillary pressure, and A is the apex of (Hg saturation/capillary pressure).0

In the Poiseuille model, the pore system is described as a bundle of tubes with various PTDs, where individual incremental diameters are summed up to give the total permeability (Purcell, 1949; Brown, 2015). Purcell’s permeability was calculated using the following equation:

$$k_{Purcell} = C f \Phi \sum_{S_{Hg}=100}^{S_{Hg}=0} \frac{S_{Hg}^i}{(P_{Hg}^i)^2} \quad (3)$$

where C is a conversion constant (14,200), f is an empirical lithology factor (0.216), Φ is the fractional porosity, S_{Hg}^i is the fractional saturation of the increment, and P_{Hg}^i is the average pressure of the increment. In this study, f was set to 0.15, which is the value proposed by Comisky et al. (2007) for tight rocks.

The best permeability estimation from MICP data for rock typing was chosen by the correlation with PDP permeability, measured in a confining stress of 7,000 psi. Recent studies have shown that MICP analysis should not be considered as an unstressed measurement due to the high isostatic pressure that mercury exerts on samples before it enters the pore system (Brown, 2015; Guise et al., 2017). The magnitude of this stress (confining stress) is equal to a threshold pressure; thus, MICP-derived permeability should be considered a permeability measured at threshold pressure (Guise et al., 2017). This statement is especially vital for tight rocks as the threshold pressure usually increases as PTD decreases. This also means that

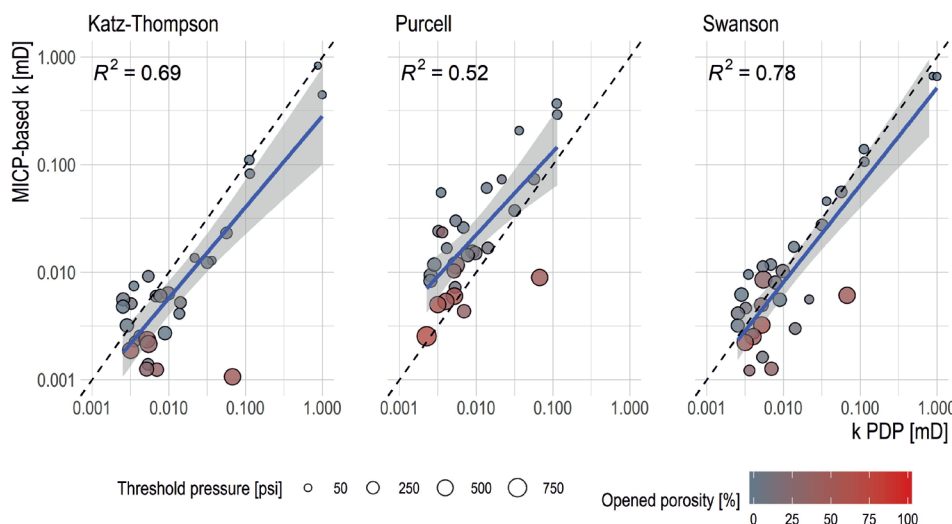


Fig. 1. Comparison of experimental PDP permeability and MICP-based permeability from the Katz–Thompson, Purcell, and Swanson models. Samples are color-coded by opened porosity. The size of the dots represents threshold pressure. The black line represents a 1:1 relationship. The blue line represents a fitted linear model with formula $y \sim x$, and the grey band represents a 95% confidence interval.

Fig. 1. Porównanie przepuszczalności PDP z przepuszczalnościami wyliczonymi z modeli Katza–Thompsona, Purcella i Swansona. Kolorami oznaczone zostały wartości porowatości otwartej. Wielkości punktów odpowiadają wartościom ciśnień progowych. Czarna, przerywana linia pokazuje relację 1:1. Niebieska linia reprezentuje dopasowany model ($y \sim x$), szara wstęga odpowiada przedziałowi ufności 95%

MICP-derived permeability for tight rock should be compared to permeability measured at high confining pressure like PDP measurement (Guise et al., 2017).

Even though the confining pressure from PDP measurement is much higher than the threshold pressure from MICP data (7,000 psi vs. a mean of 467.7 psi), the results of the permeability comparison demonstrate that MICP-derived permeability can be a useful predictor of rock permeability under simulated reservoir conditions (Fig. 1). The best match between experimental and calculated permeability was obtained for the Swanson model ($R^2 = 0.78$) (Fig. 1). Most of the PDP and Swanson permeability observations follow a 1:1 relationship. The scatter between the PDP and Swanson permeability increases slightly for samples tighter than approximately 0.01 mD. The discrepancies between those observations may stem from several factors. The PDP measures the permeability of the total pore system, which includes microfractures in addition to the matrix permeability component (Brown, 2015). The observations that lay below the 1:1 line (Fig. 1, Swanson) may have microfractures that increase PDP permeability. This fraction of permeability is not captured by the MICP method, which only estimates the matrix permeability – and, more strictly, transmissibility through the matrix pore system with cylindrical pore throats (Such and Leśniak, 2006; Brown, 2015; Guise et al., 2017). Observations that lay above the 1:1 line may be samples that are more sensitive to confining stress used in PDP measurement (7000 psi compared to MCP, between 250–500 psi). Sample heterogeneity is also possible (plugs in PDP vs. rock chips in MICP). Based on the results, Swanson permeability was chosen to represent the samples' permeability under simulation reservoir conditions, and the results from this model will be further discussed in the rock typing.

Rock typing

Rock typing based on dominant pore throat size or its fractions has been successfully applied in the differentiation of reservoir rock types within the studied formations (Skalinski et al., 2011; Skalinski and Kenter, 2014; Aliyev et al., 2016; Rabiller, 2017; Mirzaei-Paiaman et al., 2018). The approach presented in this study also utilized this idea but extended it to other petrophysical parameters that describe pore structure parameters, storage, and fluid flow potential (macro-, meso-, micro-, and nanopores, opened porosity, and Swanson permeability).

Rock types were determined using cluster analysis and the k -means method. The analysis was begun by standardizing the data that was essential to making the selected variables comparable. In order to check whether the given dataset possesses a tendency towards clusters, the Hopkins statistic test was per-

formed. The null hypothesis of the test states that the dataset is uniformly distributed (no significant clusters). The Hopkins statistics for the data was 0.08484, which allows us to reject the null hypothesis and conclude that the data is highly clustered.

The optimal number of clusters was determined using the Elbow method. This method calculates the total within-cluster sum of squares (WSS) as a function of the number of clusters ($k = 1:10$). The optimal number of clusters for the k -means method was defined, such as the one that minimizes the total intra-cluster variation (reflected in WSS) (Fig. 2). The results suggest that 4 is the optimal number of clusters (the bend in the knee in Figure 2).

K -means clustering was used to divide the samples into groups of similar pore system characteristics – known as rock types. The input data for k -means clustering are associating the opened porosity, fractions of macro-, meso-, micro-, and

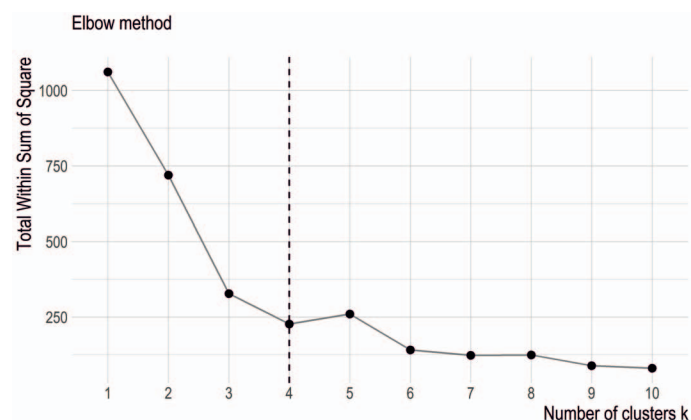


Fig. 2. The Elbow method for determining the optimal number of clusters

Fig. 2. Metoda “elbow” do wyznaczenia optymalnej liczby klastrów

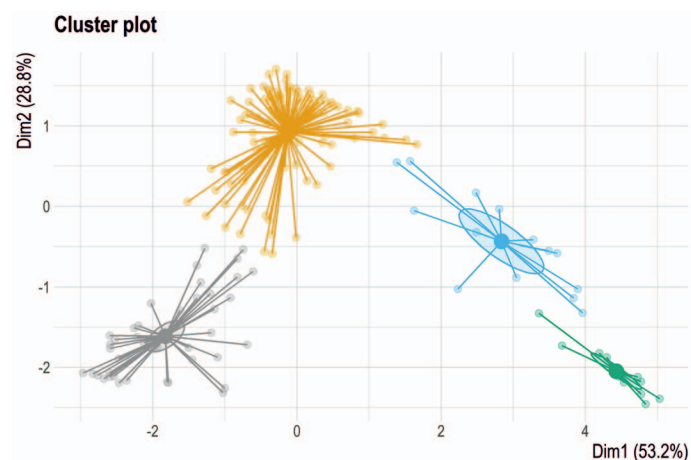


Fig. 3. Results of cluster analysis. Principal Component Analysis was used to reduce the data to two dimensions (Dim1 and Dim2)

Fig. 3. Wyniki analizy klastrowej. Analiza składowych głównych (PCA) została wykorzystana do redukcji wymiarów prezentowanych danych (dwa wymiary – Dim1 i Dim2)

nanopores, and Swanson permeability – as the parameters that best describe pore structure and fluid flow potential. All parameters were computed from MICP. The classification of observation was performed using the classical method for distance measurement using Euclidean distances and the Hartigan–Wong algorithm (Hartigan and Wong, 1979). The results of clustering are presented in a cluster plot (Fig. 3). Because there were more than two variables, a principal component analysis (PCA) was performed to reduce the number of dimensions (Dim1 and Dim2) and plot the data according to the first two principal components that explain the majority of the variance in the analyzed dataset.

The results of clustering analysis differentiated the rock types into four groups (RT1–RT4) of unique pore structure characteristics dominated by nano-, micro-, meso-, and macropores, respectively (Tab. 2, Fig. 4). This relationship is visible in Figure 5, with boxplots for individual pore fractions and other petrophysical parameters (total and opened porosity,

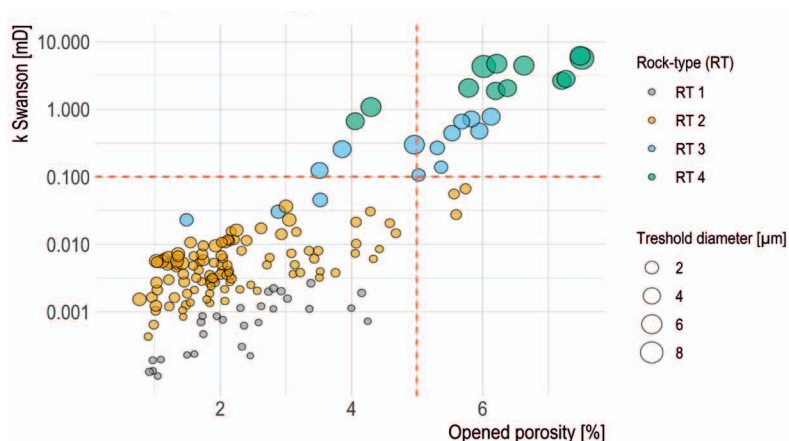


Fig. 4. Correlation between opened porosity and Swanson permeability. The samples are color-coded by RT; the size of the dots represents the threshold diameter. The dashed red horizontal line indicates the boundary between conventional and tight samples ($k = 0.1$ mD). The boundary for porosity was chosen arbitrarily (5%)

Fig. 4. Korelacja pomiędzy porowatością otwartą i przepuszczalnością Swansona. Kolorami oznaczone zostały wyznaczone klasy. Wielkości punktów reprezentują wartości średnicy progowej. Czerwona, przerywana linia horyzontalna wyznacza granice pomiędzy próbkami konwencjonalnymi i zwięzłymi ($k = 0.1$ mD). Granica dla porowatości została wyznaczona arbitralnie (5%).

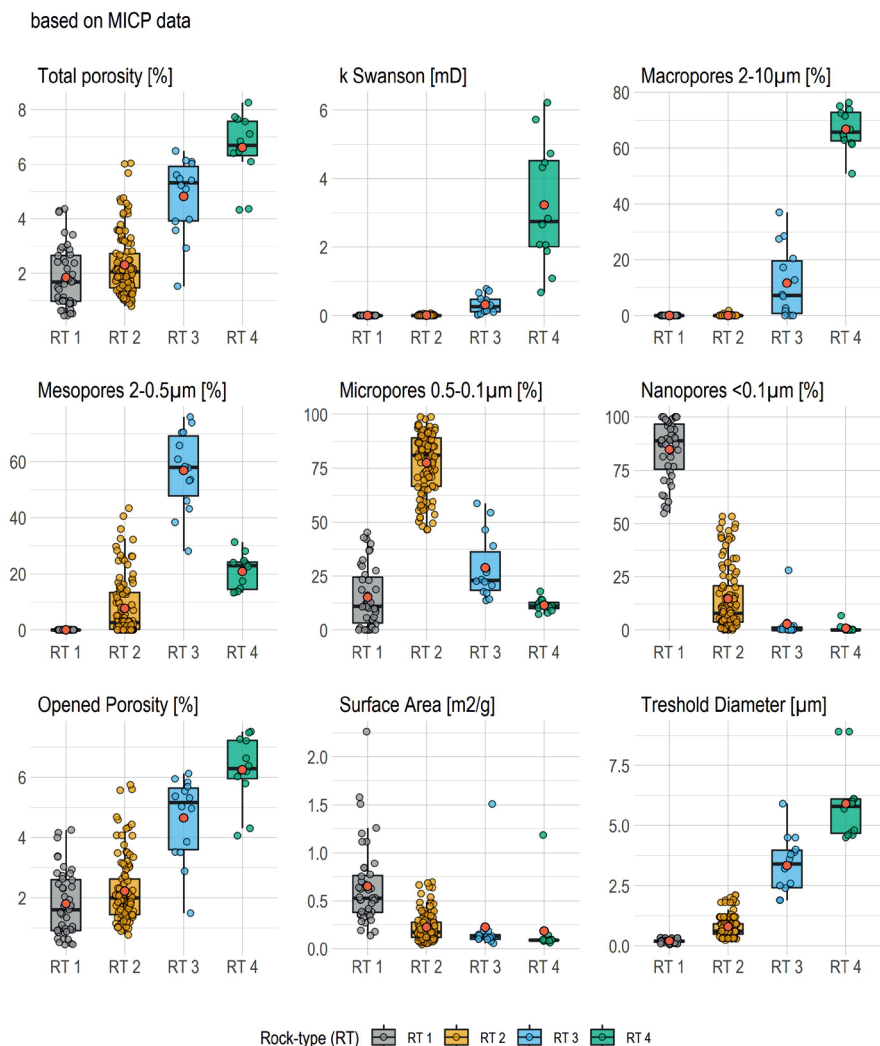


Fig. 5. Boxplots with the main pore structure parameters for individual RTs. The mean value is indicated by a red dot

Fig. 5. Wykres pudełkowy z głównymi parametrami przestrzeni porowej dla wyznaczonych klas. Wartości średniej są zaznaczone czerwonymi punktami

Table 2. Descriptive statistics for the main pore structure parameters for individual RTs**Tabela 2.** Statystyka opisowa dla głównych parametrów przestrzeni porowej w wyznaczonych klasach (RT)

	n	mean	sd	median	min	max	range	skew	kurtosis	se
RT1 (very tight)										
Total Porosity [%]	43	1.86	1.12	1.69	0.46	4.35	3.89	0.61	-0.68	0.17
Opened Porosity [%]	43	1.80	1.08	1.61	0.45	4.25	3.80	0.60	-0.73	0.17
Threshold diam. [μm]	43	0.20	0.08	0.20	0.05	0.34	0.29	0.21	-0.71	0.01
Surface area [m ² /g]	43	0.65	0.42	0.53	0.14	2.26	2.12	1.72	3.40	0.06
Macropores [%]	43	0	0	0	0	0	0	NaN	NaN	0
Mesopores [%]	43	0	0	0	0	0	0	NaN	NaN	0
Micropores [%]	43	15.17	13.87	11.10	0	45.21	45.21	0.69	-0.78	2.12
Nanopores [%]	43	84.83	13.87	88.90	54.79	100	45.21	-0.69	-0.78	2.12
k Swanson [mD]	43	0	0	0	0	0	0	1.21	0.44	0
RT2 (tight)										
Total porosity [%]	109	2.30	1.13	2.06	0.80	6.03	5.24	1.31	1.36	0.11
Opened porosity [%]	109	2.22	1.08	2.00	0.77	5.74	4.97	1.30	1.34	0.10
Threshold diam. [μm]	109	0.80	0.45	0.61	0.23	2.10	1.87	1.19	0.87	0.04
Surface area [m ² /g]	109	0.22	0.15	0.17	0.04	0.69	0.65	1.38	1.33	0.01
Macropores [%]	109	0.03	0.18	0	0	1.74	1.74	8.33	73.60	0.02
Mesopores [%]	109	7.78	10.38	2.63	0	43.33	43.33	1.45	1.31	0.99
Micropores [%]	109	77.56	13.85	81.08	46.49	98.70	52.21	-0.58	-0.79	1.33
Nanopores [%]	109	14.63	15.22	7.96	0	53.32	53.32	1.14	0.02	1.46
k Swanson [mD]	109	0.01	0.01	0	0	0.07	0.07	3.69	16.59	0
RT3 (near tight)										
Total porosity [%]	14	4.82	1.43	5.32	1.53	6.48	4.95	-0.82	-0.47	0.38
Opened porosity [%]	14	4.65	1.38	5.17	1.49	6.13	4.64	-0.84	-0.51	0.37
Threshold diam. [μm]	14	3.33	1.20	3.40	1.90	5.90	4.00	0.43	-0.85	0.32
Surface area [m ² /g]	14	0.22	0.37	0.13	0.06	1.51	1.45	2.93	7.21	0.10
Macropores [%]	14	11.60	12.50	7.15	0	36.90	36.90	0.66	-1.11	3.34
Mesopores [%]	14	56.82	14.18	57.99	28.09	75.85	47.76	-0.41	-0.99	3.79
Micropores [%]	14	28.92	14.76	22.96	13.78	58.61	44.83	0.85	-0.83	3.95
Nanopores [%]	14	2.66	7.38	0.21	0	28.07	28.07	2.89	7.04	1.97
k Swanson [mD]	14	0.31	0.26	0.26	0.02	0.78	0.76	0.52	-1.31	0.07
RT4 (conventional)										
Total porosity [%]	12	6.61	1.24	6.70	4.32	8.26	3.93	-0.69	-0.72	0.36
Opened porosity [%]	12	6.26	1.13	6.30	4.06	7.52	3.46	-0.71	-0.74	0.33
Threshold diam. [μm]	12	5.90	1.54	5.80	4.50	8.90	4.40	1.00	-0.41	0.44
Surface area [m ² /g]	12	0.18	0.32	0.09	0.06	1.18	1.12	2.63	5.42	0.09
Macropores [%]	12	66.82	7.41	65.71	50.82	76.38	25.56	-0.49	-0.66	2.14
Mesopores [%]	12	20.9	6.15	23.05	13.28	31.30	18.01	0.05	-1.53	1.78
Micropores [%]	12	11.50	2.90	11.21	7.33	17.82	10.49	0.51	-0.43	0.84
Nanopores [%]	12	0.78	1.94	0.05	0	6.78	6.78	2.43	4.64	0.56
k Swanson [mD]	12	3.23	1.82	2.74	0.67	6.22	5.55	0.23	-1.48	0.52

n – the sample size within this group; sd – standard deviation; se – the sample standard error

Swanson permeability, SSA, and threshold diameter). The first two groups (RT1–RT2) represent highly tight rocks with a Swanson permeability of <0.1 mD and a porosity of $<5\%$ (Fig. 4). Rock types 3 and 4 have more conventional characteristics, with a Swanson permeability of >0.1 mD and an opened porosity of $>5\%$.

The first group (RT1) brings together 43 samples with the lowest reservoir quality potential (low potential hydrocarbon storage capacity and low permeability) (Tab. 2, Figs. 4–6). Samples in this group are characterized by low opened porosity ranging from 0.46% to 4.35% (mean: 1.80%; median: 1.61%). In RT1, pore space is dominated by nanopores that vary from 54.79% up to 100% (mean: 84.83%; median: 88.90%); micropores account for between 0% to 45.21% (mean: 15.17%; median: 11.10%). No meso- or macropores were detected. Due to the abundance of nanopores with a pore diameter of <0.1 μm and the high value of SSA, irreducible water saturation is potentially very high, filling most of the pore space. The threshold diameters range from 0.05 to 0.34 μm (mean: 0.20 μm ; median: 0.20 μm), reflecting the highly tight character of the pore network. The PTD is characterized by a unimodal distribution with the main mode located between 0.01 μm and 0.1 μm . The Swanson permeability ranges from 0.00001 mD to 0.0026 mD (mean: 0.0006 mD; median: 0.0002 mD). Such low permeability values restrict potential fluid flow through the formation.

The second group (RT2) is the largest group, including 109 samples with low reservoir quality potential (Tab. 2, Figs. 4–6). The opened porosity of RT2 varies from 0.77% to 5.74% (mean: 2.22%; median: 2.0%), which makes it similar to RT1. However, in contrast to RT1, RT2 is dominated by micropores that constitute 46.49% up to 98.70% of the pore space (mean: 77.56%; median: 81.08%). Nanopores range from 0% to 53.32% (mean: 14.63%; median: 7.96%). Mesopores range from 0% to 43.33% (mean: 7.78%; median: 2.63%), while macropores reach a maximum of 1.74%. Threshold diameters range from 0.23 to 2.1 μm (mean: 0.80 μm ; median: 0.61 μm). The PTD is similar to RT1 but with a main mode shifted towards larger pore throats (0.1–0.5 μm). The Swanson permeability ranges from 0.0004 mD to 0.0665 mD (mean: 0.0076 mD; median: 0.0049 mD).

The third group (RT3) unites 14 samples with moderate reservoir quality potential (Tab. 2, Figs. 4–6). The opened porosity of RT3 ranges from 1.49% to 6.13% (mean: 4.65%; median: 5.17%). Pore space is divided mainly between mesopores – 28.09% to 75.85% (mean: 56.82%; median: 57.99%) – and micropores – 13.78% to 58.61% (mean: 28.92%; median: 22.96%). The proportion of macropores varies from 0% to 36.90% (mean: 11.60%; median: 7.15%), while that of nanopores varies between

0% and 28.07% (mean: 2.66%; median: 0.21%). Threshold diameter ranges from 1.90 μm to 5.90 μm (mean: 3.33 μm ; median: 3.40 μm). Most of the samples from RT3 have bimodal PTD with various distribution of peaks between 0.5 μm and 2 μm . The Swanson permeability ranges from 0.2960 mD to 0.7798 mD (mean: 0.3125 mD; median: 0.2624 mD).

The fourth group (RT4) brings together 12 samples with good reservoir quality potential (Tab. 3, Fig. 5). Opened porosity ranges from 4.32% to 7.52% (mean: 6.26%; median: 6.30%). Pore space is dominated by macropores that range from 50.82% to 76.38% (mean: 66.82%; median: 65.71%). Mesopores range from 13.28% to 31.30% (mean: 20.90%; median: 23.05%). The micropores take up from 7.33% to 17.82% (mean: 10.15%; median: 11.21%) of the pore space, while nanopores fill up to 6.78%. The pore structure characteristics of RT4 keeps the potential irreducible water saturation at a very low level. The threshold diameter varies between 4.50 μm and 8.90 μm (mean: 5.90 μm ; median: 5.80 μm). This threshold diameter, along with the high proportion of macropores, provides a well-developed pore network system for the fluid flow. The PTD is characterized by a unimodal distribution with the main sharp peak between 2 and 6 μm . The Swanson permeability ranges from 0.6670 mD to 6.2201 mD (mean: 3.2268 mD; median: 2.7434 mD).

The differences in the pore structure between designated RTs were also captured by computer analysis of microscopic images (CAMI) using the procedure described by Leśniak (1999). The CAMI analysis was performed on four selected thin-sections, each representing an individual RT in terms of mean porosity (Fig. 6).

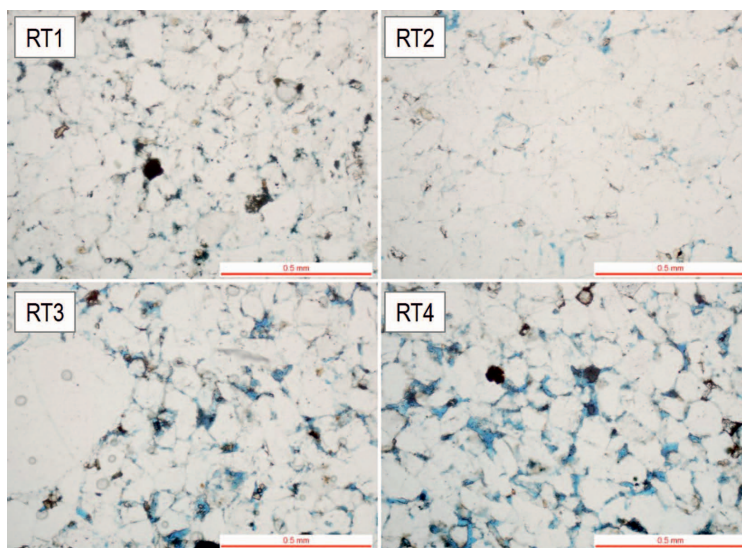
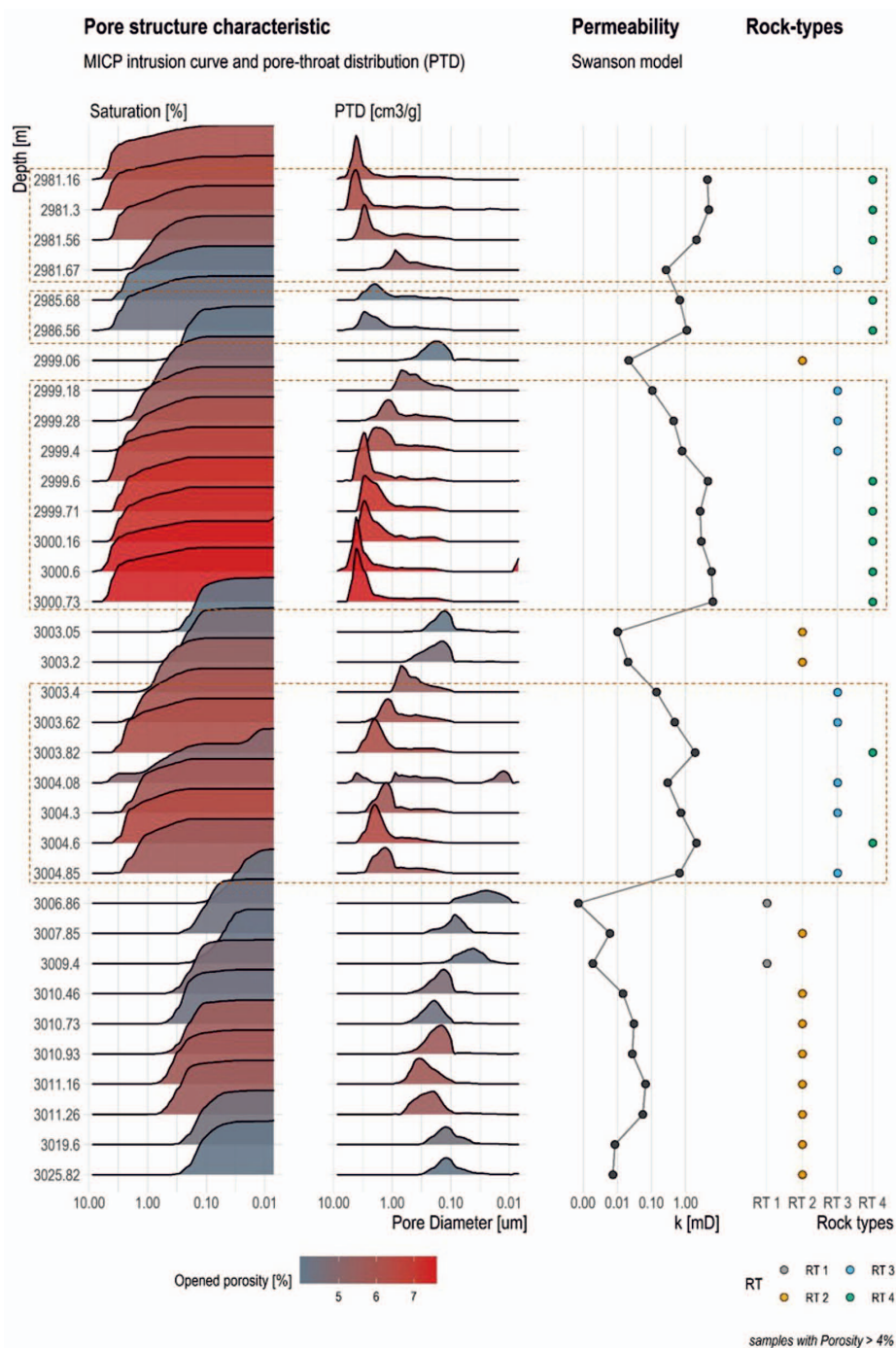


Fig. 6. Microscopic images of four selected samples from individual RTs. The samples were impregnated with blue epoxy in order to identify porosity

Fig. 6. Zdjęcia mikroskopowe dla czterech wyselekcjonowanych próbek z wydzielonych typów skał. W celu identyfikacji porowatości, próbki zostały nasycone niebieską żywicą

Table 3. Proportions of pore sizes from CAMI for selected specimens representing individual RTs**Tabela 3.** Procentowe udziały wielkości porów z CAMI dla czterech wyselekcjonowanych próbek reprezentujących różne typy skał

Pore size [mm]	Proportion [%]			
	RT1	RT2	RT3	RT4
< 0.01	78.54	69.74	62.97	59.55
0.01–0.02	15.23	20.68	23.41	21.02
0.02–0.03	3.90	5.48	8.21	9.56
0.03–0.04	1.44	2.16	3.08	4.48
0.04–0.05	0.58	0.97	1.26	2.36
0.05–0.06	0.16	0.54	0.66	1.18
0.06–0.07	0.08	0.16	0.23	0.74
> 0.07	0.08	0.27	0.19	1.11

**Fig. 7.** Integration of the data into an array log. From the left: pore structure characteristics with saturation and PTD curves (curves were smoothed using the loess function; the areas underneath the curves are color-coded by opened porosity), Swanson permeability, and rock types. Rectangles mark the most promising intervals**Fig. 7.** Integracja danych w funkcji głębokości. Od lewej charakterystyka struktury porów z krzywymi nasycenia Hg i rozkładem średnic porów (krzywe zostały wygładzone przy użyciu funkcji loess; obszar pod wykresem został pokolorowany przy użyciu wartości porowatości otwartej), przepuszczalność Swansona, wyznaczone klasy. Obszary zaznaczone prostokątami wskazują interwały o najbardziej perspektywicznych parametrach petrofizycznych

sample is also very low, equaling 0.0095 mm. The CAMI results from the sample belonging to RT3 showed better connectivity and higher pore length and width, with a mean equivalent pore diameter equal to 0.0107 mm. The sample from RT4 is characterized by the greatest length, width, and pore connectivity, and a mean equivalent pore diameter of 0.0128 mm (Tab. 3). The differences between the analyzed pore spaces for individual RTs are also visible in the percentages of specified pore fractions (Tab. 3). The proportion of mean equivalent pore diameters below 0.02 mm were 93.7%, 90.4%, 86.4%, and 80.6% for RT1, RT2, RT3, and RT4, respectively. The sample from RT4 stands out against the others with its high content of pores with a mean equivalent diameter above 0.07 mm (from 4 to 17 times higher than the other RTs).

The final step in the workflow involves the integration of all computed MICP data that govern reservoir storage and fluid flow potential (MICP saturation, MICP PTD, and permeability) into the array log. The resulting data demonstrate that the most promising intervals are located at 2981.16–2981.67 m, 2985.68–2986.56 m, 2999.18–3000.73 m, and 3003.4–3004.8 m, and include rocks belonging to RT3 and RT4 (Fig. 7).

Conclusions

This study demonstrates the workflow used to characterize rock types according to pore structure characteristics that determine storage and fluid flow potential in a tight-sand reservoir. The rock types were determined using the machine learning *k*-means method on user-defined parameters, including opened porosity, proportions of macro-, meso-, micro-, and nanopores, and Swanson permeability – all information obtained from MICP measurement. The comparison between Swanson and PDP permeabilities revealed that MICP-derived permeability could be a useful estimation of rock permeability under simulated reservoir conditions. Cluster analysis revealed four groups – rock types – of unique pore structure characteristics that significantly differ in macro-, meso-, micro-, and nanopore content. Rock types 1 and 2 were designated as highly tight, unconventional reservoirs (a Swanson permeability of <0.1 mD and a porosity of <5%), while rock types 3 and 4 showed more conventional characteristics (a Swanson permeability of >0.1 mD and an opened porosity of >5%). The variability in the pore structure between designated rock types was also captured using CAMI. Integrating the data into the array log helped identify the intervals with the most promising reservoir parameters. These intervals are located at 2981.16–2981.67 m, 2985.68–2986.56 m, 2999.18–3000.73 m, and 3003.4–3004.8 m.

Acknowledgments

The author thanks Polskie Górnictwo Naftowe i Gazownictwo (PGNiG SA) for permission to use the archival MICP data. The author also thanks Dr. Grzegorz Leśniak for CAMI analysis and Prof. Piotr Such for valuable comments.

This paper was written on the basis of the statutory work entitled: *Pore-typing w formacjach zwięzłych piaskowców* (Pore-typing in tight-gas sandstone) – the work of the Oil and Gas Institute – National Research Institute was commissioned by the Ministry of Science and Higher Education; order number: 0058/SG/2019, archival number: DK-4100/0048/2019.

References

- Aliyev E., Saidian M., Prasad M., Russell B., 2016. Rock typing of tight gas sands. A case study in Lance and Mesaverde formations from Jonah field. *Journal of Natural Gas Science and Engineering*, 33:1260–1270. DOI:10.1016/j.jngse.2015.12.045.
- Amaefule J.O., Altunbay M., Tiab D., Karsey D.G., Keelan D., 1993. Enhanced Reservoir Description: Using Core and Log Data to Identify Hydraulic (Flow) Units and Predict Permeability in Uncored Intervals/Wells. *Society of Petroleum Engineers*. DOI: SPE-26436-MS.
- Archie G.E., 1950. Introduction to Petrophysics of Reservoir Rocks. *AAPG Bulletin*, 34: 943–961. <http://archives.datapages.com/data/bulletns/1949-52/data/pg/0034/0005/0900/0943.htm?doi=10.1306%2F3D933F62-16B1-11D7-8645000102C1865D> (accessed: October 2019).
- Brown A.A., 2015. Interpreting Permeability from Mercury Injection Capillary Pressure Data: *AAPG Annual Convention and Exhibition, Denver, Colorado, 31 May–3 June 2015*, 41660: 3–5.
- Comisky J.T., Newsham K., Rushing J.A., Blasingame T.A., 2007. A Comparative Study of Capillary-Pressure-Based Empirical Models for Estimating Absolute Permeability in Tight Gas Sands: *Society of Petroleum Engineers*. DOI:10.2118/110050-MS.
- Dolson J., 2016. Understanding oil and gas shows and seals in the search for hydrocarbons. *Springer*, 1–486. DOI: 10.1007/978-3-319-29710-1.
- Guise P., Grattoni C., Fisher Q.J., Schiffer A., 2017. Stress Sensitivity of Mercury. *International Symposium of the Society of Core Analysts, Vienna, Austria, 27–30 August 2017*, 1–12.
- Hartigan J.A., Wong M.A., 1979. Algorithm AS 136: A K-Means Clustering Algorithm. https://www.labri.fr/perso/bpinaud/userfiles/downloads/hartigan_1979_kmeans.pdf (accessed: May 2019).
- Jones S.C., 1997. A Technique for Faster Pulse-Decay Permeability Measurements in Tight Rocks. *SPE Formation Evaluation*, 12:19–26. DOI: 10.2118/28450-PA.
- Katz A.J., Thompson A.H., 1987. Prediction of Rock Electrical Conductivity from Mercury Injection Measurements. *Journal of Geophysical Research*, 92: 599–607.
- Kennedy R.L., Knecht W.N., Georgi D.T., 2012. Comparisons and Contrasts of Shale Gas and Tight Gas Developments, North American Experience and Trends. *Society of Petroleum Engineers*. DOI: 10.2118/160855-MS.
- Krakowska P., Puskarczyk E., Habrat M., Madejski P., Jędrychowski M., 2018. Parametry geometryczne przestrzeni porowej niskoporo- watyh piaskowców kambryjskich wyznaczone na podstawie wyników badań laboratoryjnych na próbkach z rdzeni wiertni- czych. *Nafta-Gaz*, 11:783–788. DOI: 10.18668/NG.2018.11.01.
- Lan Y., Davudov D., Ghanbarnezhad Moghanloo R., 2017. Interplay between permeability and compressibility in shale samples.

- Journal of Petroleum Science and Engineering*, 159: 644–653. DOI:10.1016/j.petrol.2017.09.072.
- Law B.E., Curtis J.B., 2002. Introduction to Unconventional Petroleum Systems: *AAPG Bulletin*, 86: 1851–1852. DOI: 10.1306/61EEDDA0-173E-11D7-8645000102C1865D.
- Leśniak G., 1999. Application of computer analysis of microscopic images in petrophysical investigations. *Przegląd Geologiczny*, 47: 644–651.
- Ma Y.Z., Moore W.R., Gomez E., Clark W.J. and Zhang, Y., 2015. Tight Gas Sandstone Reservoirs, Part 1: Overview and Lithofacies. *Elsevier Inc.*, 405–427. DOI: 10.1016/B978-0-12-802238-2.00014-6.
- Mirzaei-Paiaman, A., Ostadhassan, M., Rezaee, R., Saboorian-Jooybari, H., and Chen, Z., 2018. A new approach in petrophysical rock typing. *Journal of Petroleum Science and Engineering*, 166:445–464. DOI: 10.1016/j.petrol.2018.03.075.
- Naik G.C., 2005. Tight Gas Reservoirs – An Unconventional Natural Energy Source for the Future. 1–32.
- Pittman E.D., 1992. Estimating Pore Throat Size in Sandstones from Routine Core-Analysis Data). *AAPG Bulletin*, 76: 191–198. <http://www.searchanddiscovery.com/documents/pittman/> (accessed: May 2019).
- Purcell W.R., 1949. Capillary Pressures – Their Measurement Using Mercury and the Calculation of Permeability Therefrom. *Journal of Petroleum Technology*, 1: 39–48. DOI: 10.2118/949039-G.
- R Core Team, 2018. R: A Language and Environment for Statistical Computing. *R Foundation for Statistical Computing. Vienna*. <https://www.r-project.org>.
- Rabiller P., 2017. Combining porosimetry and Purcell permeability modeling to calibrate FZI and define a dynamic permeability cut off. *Society of Core Analysts*, 1–9.
- Rushing J.A., Newsham K.E., Blasingame T.A., 2008. Rock Typing: Keys to Understanding Productivity in Tight Gas Sands. *Society of Petroleum Engineers*. DOI: 10.2118/114164-MS.
- Skalinski M., Kenter J.A., Jenkins S., Tankersley T., 2011. Updated Rock Type Definition and Pore Type Classification of a Carbonate Buildup, Tengiz Field, Republic of Kazakhstan (Russian). *Society of Petroleum Engineers*. DOI: 10.2118/139986-ru.
- Skalinski M., Kenter J.A.M., 2014. Carbonate petrophysical rock typing: integrating geological attributes and petrophysical properties while linking with dynamic behaviour: *Geological Society, London, Special Publications*, 406: 229–259. DOI: 10.1144/sp406.6.
- Such P., Leśniak G., 2003. Parametry przestrzeni porowej skał. Kraków, *Prace Instytutu Górnictwa Naftowego i Gazownictwa*, 119: 63.
- Such P., Leśniak G., 2006. Warunki konieczne i wystarczające dla up-scalingu danych petrofizycznych. *Nafta-Gaz*, 11: 565–570.
- Such P., Leśniak G., Budak P., 2007. Kompleksowa metodyka badania właściwości petrofizycznych skał. *Prace Instytutu Górnictwa Naftowego i Gazownictwa*, 142: 69.
- Swanson B.F., 2007. A Simple Correlation Between Permeabilities and Mercury Capillary Pressures. *Journal of Petroleum Technology*, 33: 2498–2504. DOI: 10.2118/8234-pa.
- Washburn E.W., 1921. Note on a Method of Determining the Distribution of Pore Sizes in a Porous Material. *Proceedings of the National Academy of Sciences of the United States of America*, 7: 115–6. DOI: 10.1073/pnas.7.4.115.
- Webb P.A., 2001. An Introduction to the Physical Characterization of Materials by Mercury Intrusion Porosimetry with Emphasis on Reduction and Presentation of Experimental Data. *Micromeritics Instrument Corp.*, 22: 1–23. DOI: 10.1177/004057368303900411.



Tomasz TOPÓR, PhD
 Head of Petrophysics Laboratory
 Department of Geology and Geochemistry
 Oil and Gas Institute – National Research Institute
 Lubicz 25 A
 31-503 Krakow
 E-mail: toport@inig.pl